Applied Physics Letters

Continuously tunable radio frequency electrometry with Rydberg atoms

Cite as: Appl. Phys. Lett. **121**, 014002 (2022); https://doi.org/10.1063/5.0086357
Submitted: 25 January 2022 • Accepted: 23 June 2022 • Published Online: 07 July 2022

Jinlian Hu, Huaqiang Li, Rong Song, et al.

Applied Physics Letters ARTICLE scitation.org/journal/apl

Continuously tunable radio frequency electrometry with Rydberg atoms

Cite as: Appl. Phys. Lett. **121**, 014002 (2022); doi: 10.1063/5.0086357
Submitted: 25 January 2022 · Accepted: 23 June 2022 ·
Published Online: 7 July 2022

Jinlian Hu,[1] Huaqiang Li,[1] Rong Song,[1] Jingxu Bai,[1] Yuechun Jiao,[1,2,a)] Jianming Zhao,[1,2,a)] and Suotang Jia[1,2]

AFFILIATIONS

[1]State Key Laboratory of Quantum Optics and Quantum Optics Devices, Institute of Laser Spectroscopy, Shanxi University, Taiyuan 030006, People's Republic of China
[2]Collaborative Innovation Center of Extreme Optics, Shanxi University, Taiyuan 030006, China

[a)]**Authors to whom correspondence should be addressed:** ycjiao@sxu.edu.cn and zhaojm@sxu.edu.cn

ABSTRACT

We demonstrate a continuously tunable electric field measurement based on the far off-resonant AC stark effect in a Rydberg atomic vapor cell. In this configuration, a strong far off-resonant field, denoted as a local oscillator (LO) field, acts as a gain to shift the Rydberg level to a high sensitivity region. An incident weak signal field with a few hundreds of kHz difference from the LO field is mixed with the LO field in the Rydberg system to generate an intermediate frequency signal, which is read out by Rydberg electromagnetically induced transparency (Rydberg-EIT) spectroscopy. Not like resonant EIT-Autler–Townes spectra, we realize the electric field measurement of the signal frequency from 2 to 5 GHz using a single Rydberg state. The detectable field strength is down to 2.25 μV/cm with sensitivity of the electrometry 712 nV cm^{-1} Hz$^{-1/2}$, and a linear dynamic range is over 65 dB. The detectable field strength is comparable with a resonant microwave-dressed Rydberg heterodyne receiver using the same system, which is 0.96 μV/cm with sensitivity of 304 nV cm^{-1} Hz$^{-1/2}$. We also show the system has an inherent polarization selectivity feature. Our method can provide high sensitivity of electric field measurement and be extended to arbitrary frequency measurements.

Atom-based sensing has unique advantages in the measurement of weak signals with high sensitivity, calibration-free, and intrinsic accuracy. Seminal advances include atomic clocks[1] and magnetometers.[2] A quantum sensor for the radio frequency (RF) field is also expected to follow because of its widespread application.

A significant progress has been made in the atom-based measurement of RF electric fields using Rydberg atoms due to their large dc polarizabilities and microwave-transition dipole moments.[3] Optical Rydberg electromagnetically induced transparency (Rydberg-EIT) spectroscopy and Autler–Townes (AT) splitting have been employed to measure the RF field over a wide frequency range from 100 MHz (Refs. 4 and 5) to over 1 THz,[6] including the measurement of the strength of the RF field and polarizations,[7–9] the sub-wavelength microwave imaging,[10,11] and the first demonstration of angle-of-arrival measurements.[12] The concept of the wireless communication recently based on Rydberg atoms also has been demonstrated, including amplitude modulation (AM),[13–15] frequency modulation (FM),[16] and phase modulation (PM).[17,18] Recently, the sensitivity of the Rydberg atomic sensor is greatly improved to 55 nV cm^{-1} Hz$^{-1/2}$ (Refs. 19 and 20) using a heterodyne receiver architecture and later to 30 nV cm^{-1} Hz$^{-1/2}$ by using an optical ground-state repumping technique.[21] However, the above-mentioned works have relied on resonant or near-resonant transitions between Rydberg states, which restricts any measurement of RF fields to a discrete set of atomic transition frequencies from ∼ GHz to ∼ THz with a bandwidth less than 10 MHz. Using all of the available transitions requires a laser system with broad tunability or a multiple laser system realizing frequency stabilization to atomic transitions, which is complex and expensive. To achieve continuous radio frequency electric-field detection with high sensitivity, a dressing field resonant with an adjacent Rydberg transition in a five-level atomic scheme is applied to shift the Rydberg levels, which allows for the detection of frequencies in a continuous band between resonances with adjacent Rydberg states.[22] Distinct from the resonant EIT-AT method, a sensor based on the AC Stark shift can achieve a continuously tunable electric field measurement with a single Rydberg state. The proof-of-principle experiment indicates that the Rydberg sensor can achieve the continuous-frequency measurement for sufficiently strong electric fields from 200 V/m to >1 kV/m.[23,24] For the

weak electric field with continuous frequency, an off resonance heterodyne technique is utilized to greatly boost the sensitivity at arbitrary frequencies in the waveguide-coupled Rydberg system,[25] while it is not likely to achieve absolute electric field accuracy, which outperforms previous free-space Rydberg electric field measurements.

In this work, we present an AC-Stark based weak RF electric field measurement technique with the RF frequency from 2 to 5 GHz using one Rydberg level in a vapor cell filled with ^{133}Cs atoms. The basic idea is that a strong far off-resonant field is introduced as a local oscillator (LO) field to AC Stark shift the Rydberg level to the high sensitivity point. Specifically, we choose a $|60D_{5/2}\rangle$ state that exhibits m_j-dependent AC stark shifts and splits in the presence of a strong LO field. We lock the laser frequency to a big slope point of the $m_j = 1/2$ Stark level because of its larger polarizability than that of $m_j = 5/2, 3/2$. The incident weak signal field, mixed with the LO field in the Rydberg system, is read out by Rydberg-EIT. The readout signal is linearly dependent on the strength of the signal field with a dynamic range over 65 dB, and the detectable field strength is down to 2.25 μV/cm with a sensitivity of 712 nV cm^{-1} Hz$^{-1/2}$, which is comparable with a resonant RF-dressed Rydberg heterodyne receiver, achieving 0.96 μV/cm with a sensitivity of 304 nV cm^{-1} Hz$^{-1/2}$ using the same experimental system. We also show the polarization detection of the RF field, corresponding isolation ratio for two orthogonal signal fields being up to 32 dB. Our method, in principle, provides the RF electric field measurement at arbitrary frequencies with high sensitivity.

The experimental setup and the relevant ^{133}Cs Rydberg-EIT three-level diagram are illustrated in Fig. 1. A Rydberg coupling laser ($\lambda_c = 510$ nm) and a probe laser ($\lambda_p = 852$ nm) counter-propagate through a cylindrical room-temperature cesium cell with 50 mm long and 20 mm diameter, where the probe beam with a $1/e^2$ waist radius of 500 μm and a power of 200 μW is locked to the transition of $|6S_{1/2}(F = 4)\rangle \rightarrow |6P_{3/2}(F' = 5)\rangle$ using modulation transfer spectroscopy,[26] and the coupling laser with a $1/e^2$ waist radius of 550 μm and a power of 18.5 mW further excites the atoms to the Rydberg state $|60D_{5/2}\rangle$, thus establishing the EIT to enhance the probe transmission. The EIT signal is detected by measuring the transmission of the probe laser using a photodiode (PD). A reference beam, separated from the probe laser beam, is subtracted with the transmitted EIT signal to eliminate any probe laser power drift. The probe and coupling lasers keep co-linear polarization along the y-axis.

Two radio frequency fields with the co-linear polarization along the y-axis, denoted as a local oscillator (LO) field E_{LO} and a weak signal fields E_{Sig}, are incident to the Rydberg system simultaneously. The LO field operated at a frequency of 2.180 GHz (SRS SG386), which is far off-resonant with the transition of $|60D_{5/2}\rangle$ to an adjacent $|61P_{3/2}\rangle$ Rydberg state, and emitted from a horn antenna (A-info LB-20180-SF). Under the strong LO field, the $|60D_{5/2}\rangle$ Rydberg state exhibits m_j-dependent ($m_j = 1/2, 3/2, 5/2$) AC Stark shifts and splits, shown in the below of Fig. 1(a). The slope of the $m_j = 1/2$ Stark level is much larger than that of zero field, which means the $m_j = 1/2$ Stark level is more sensitive to the electric field. The weak signal field with 75 kHz frequency difference of the LO field is generated with the other signal generator and emitted with the other identical horn antenna.

When the LO field (E_{LO}) and the signal field (E_{Sig}) are incident on the vapor cell, the response of the Rydberg atom to both fields is described in detail in Ref. 25. Here, we give the simplified results.

For the near resonant field of the Autler–Townes regime, the total RF electric field (E_{tot}) that the atoms feel can be expressed as

$$E_{tot} \approx E_{LO}/2 + E_{Sig}/2\cos(\Delta\omega + \Delta\phi), \quad (1)$$

and the Autler–Townes splitting is given by

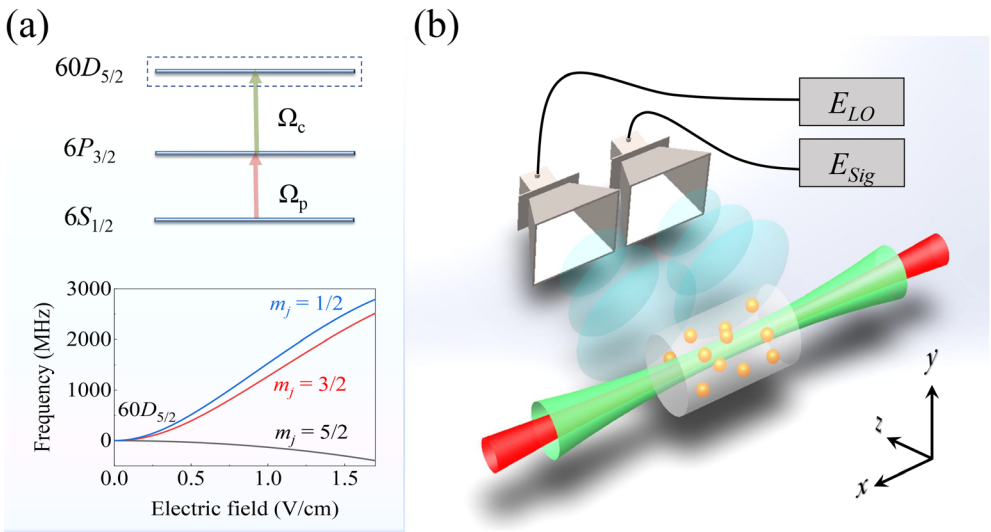

FIG. 1. (a) Top: energy-level diagram of the three-level Rydberg-EIT of a cesium atom. A probe laser, Ω_p ($\lambda_p = 852$ nm), is resonant with the lower transition $|6S_{1/2}(F = 4)\rangle \rightarrow |6P_{3/2}(F' = 5)\rangle$, and a coupling laser Ω_c ($\lambda_c = 510$ nm) couples the transition of $|6P_{3/2}(F' = 5)\rangle \rightarrow |60D_{5/2}\rangle$. Below: Stark spectra of the Rydberg state $|60D_{5/2}\rangle$. With increasing the strength of field, the energy level shifts and splits into three Stark levels, $|m_j = 5/2\rangle$ (black line), $|m_j = 3/2\rangle$ (red line), and $|m_j = 1/2\rangle$ (blue line). (b) Sketch of the experimental setup. A coupling laser and a probe laser counter-propagate through a cylindrical room-temperature cesium cell. The transmission of the probe laser is detected using a photodiode (PD). A reference beam (not shown in here), separated from the probe laser beam, is subtracted with the transmission probe laser to eliminate any probe laser power drift. A LO field E_{LO} and a weak signal field E_{Sig} are emitted from two identical horn antennas.

$$\Delta f_{AT} = \frac{\mu}{h} E_{tot}, \tag{2}$$

where $E_{LO}(E_{Sig})$, $\omega_{LO}(\omega_{Sig})$, and $\phi_{LO}(\phi_{Sig})$ represent the amplitude, angular frequency, and phase of the local oscillation field (signal field), respectively. $\Delta\omega$ is the difference between the angular frequency of the local field and the signal field, $\Delta\omega = \omega_{LO} - \omega_{Sig} \ll \bar{\omega} = (\omega_{LO} + \omega_{Sig})/2$. $\Delta\phi$ is the difference between the phase of the local field and the signal field, $\Delta\phi = \phi_{LO} - \phi_{Sig}$. Δf_{AT} is the RF field dressed Autler–Townes splitting, h is the Planck constant, and μ is the transition matrix element between two Rydberg states.

For the far off-resonant of the Stark shift regime, the total field of the Rydberg atoms experienced becomes

$$E_{tot}^2 \approx E_{Sig}^2/2 + E_{LO}^2/2 + E_{Sig}E_{LO}\cos(\Delta\omega + \Delta\phi), \tag{3}$$

and the Stark shift of the Rydberg state depends on the atomic polarizability. Since the RF-field frequency here is much lower than the Kepler frequency (35 GHz for Cs 60D), the AC Stark shifts can be written as[4,5,27]

$$\Delta f_{stark} = -\frac{1}{2}\alpha\langle E_{tot}^2\rangle, \tag{4}$$

where Δf_{stark} is the Stark shift, α represents the dc polarizabilities of the $|60D_{5/2}, m_j\rangle$ states, and $\langle E_{tot}^2\rangle$ is the average value of the square of the electric field.

In both cases, the Rydberg-EIT signal varies at a frequency of $\Delta\omega/2\pi$, and the related amplitude is linearly proportional to the signal field E_{Sig}. Especially, under the far off-resonant case, the LO field E_{LO} acts as a gain to amplify the signal field, shown with the last term of Eq. (3). In Fig. 2(a), we demonstrate Rydberg-EIT spectra for the $|60D_{5/2}\rangle$ state without a RF field (the top curve), with only the LO field (the middle curve), and with both the strong LO field and the weak signal (the bottom curve). The LO field is $E_{LO} = 0.18$ V/cm with the frequency of $f_{LO} = 2.180$ GHz, whereas the signal field is $E_{Sig} = 7.23$ mV/cm with the frequency of $f_{Sig} = 2.180\,075$ GHz, having a fixed frequency difference of $\delta = 75$ kHz. It is clearly shown that in the presence of the local field, the EIT spectrum shows energy shifts and splits into three peaks, denoted as $m_j = 1/2$, 3/2, 5/2, as shown with the middle curve. When both the LO field and the weak signal interact with atoms, we can observe the Rydberg-EIT line broadening, as shown with the bottom curve of Fig. 2(a). The $m_j = 1/2$ Stark spectrum exhibits a maximal broadening compared to the $m_j = 5/2$, 3/2 Stark lines due to the larger polarizability of the $m_j = 1/2$ line, see the enlargement of the square marked region in Fig. 2(c). This EIT line broadening is attributed to the beat signal between the LO field and the signal field.[28] From Eq. (3), the weak signal, E_{Sig}, can be obtained by analyzing the modulated EIT spectrum with a spectrum analyzer (ROHDE & SCHWARZ FSVA13).

In order to measure the weak signal field, the center of the $m_j = 1/2$ Stark line is chosen as the 510 nm laser frequency operating point forming Rydberg EIT. In Fig. 2(b), we present the output strength of our Rydberg sensor, where we measure the output signal of the spectrum analyzer for different power of the LO field and fixed signal field $E_{Sig} = 0.73$ mV/cm. We can see the LO field has an optimal operating point, where the system is the most sensitivity for the signal field. In the following, we fix the strength of the LO field operating at the optimal point $E_{LO} = 0.21$ V/cm. A similar result is obtained in a

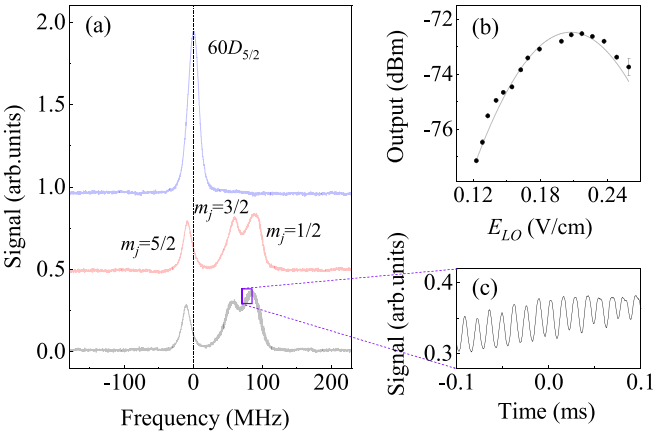

FIG. 2. (a) Rydberg-EIT spectra for the $|60D_{5/2}\rangle$ state without a RF field (the top curve), with only a LO field (the middle curve), and with both the strong LO field and a weak signal simultaneously (the bottom curve). The main peak at near 0 detuning is formed by the cascade three-level atom of $|6S_{1/2}(F=4)\rangle \rightarrow |6P_{3/2}(F'=5)\rangle \rightarrow |60D_{5/2}\rangle$, marked with a dashed line. The detuning axis is calibrated by the $|60D_J\rangle$ fine-structure splitting, and the ($|60D_{3/2}\rangle$ EIT peak is not shown here).[4] In the presence of the LO field, the EIT spectrum shows energy shifts and splits into three peaks due to AC Stark effects, denoted as $m_j = 1/2$, 3/2, and 5/2. When both the LO field and signal field are incident, the EIT spectrum further shows amplitude-modulation at frequency $\Delta\omega/2\pi$ on the spectrum line. A maximal amplitude-modulated response appears at the $m_j = 1/2$ Stark level due to its larger polarizability. (b) The response of the system to the LO field with fixed signal field. (c) The zoomed part for the spectrum of the $m_j = 1/2$ Stark level in the time domain, which is convenient to show the modulation frequency of $\Delta\omega/2\pi = 75$ kHz.

resonant EIT-AT regime,[29] but its optimal LO field operating point is much smaller than our work as the AC Stark effect occurs under a strong electric field.

We then lock the probe laser to the transition $|6S_{1/2}(F=4)\rangle \rightarrow |6P_{3/2}(F'=5)\rangle$ and the coupling laser to the most sensitivity peak at $m_j = 1/2$ to measure the response of system to the signal field. The inset of Fig. 3(a) presents the measured transition of the probe laser for three indicated signal fields E_{Sig}. As mentioned above, the transmitted EIT signal shows a sinusoidal profile with the frequency $\delta = 75$ kHz, and the amplitude of the sinusoidal curve increases with signal field power. We measure the amplitude of signal fields as a function of the RF power P at the horn antenna using the spectrum analyzer with a resolution bandwidth of 10 Hz (the measurement time of T = 0.1 s) and a video bandwidth of 1 Hz. The results are shown as black dots in Fig. 3(a), and the output of the spectrum analyzer linearly increases with the RF power P. To calibrate the signal field values, we measure Stark shifts of energy at a strong field region, in which the E_{tot}^2 is proportional to the RF power P, as expected in Eq. (4). The measured electric field is shown with red dots in Fig. 3(a). The E-field strength at a distance of 14 cm from the Rydberg sensor was calculated using

$$E^2 = F^2\frac{30P \cdot g}{d^2}, \tag{5}$$

where E is the electric field, g is a gain factor of the antenna, d is the distance between the horn antenna port and the center of the cesium cell, and F is the cell perturbation factor, which can be determined

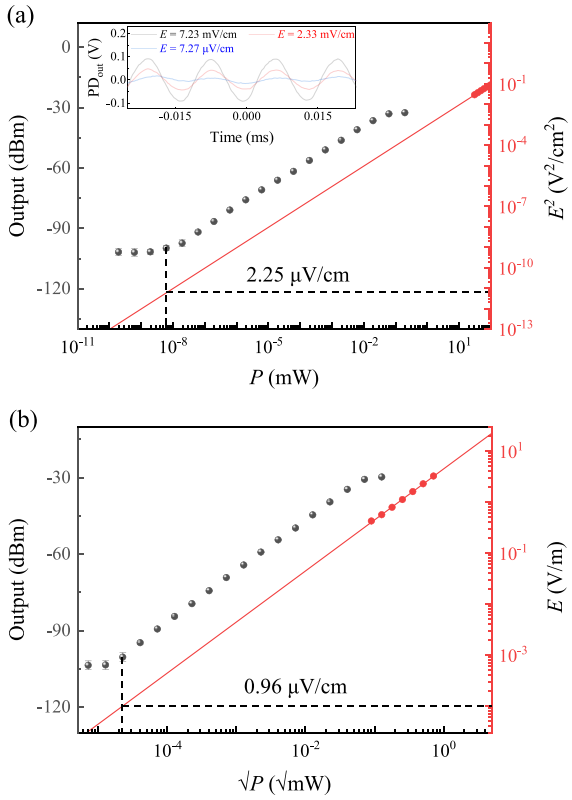

FIG. 3. (a) Measurement of the weak signal field using the AC Stark technique with $f_{LO} = 2.180$ GHz and $\delta = 75$ kHz. The data are taken with the far off-resonant AC stark heterodyne technique (black dots) and with the AC Stark shift in the strong regime (red dots). The red solid line displays the electric field calculated in Eq. (5). The dashed line shows the detectable electric field of $E_{det} = 2.25\ \mu$V/cm. Inset: the probe laser transmission at the time domain for three indicated signal fields E_{Sig} with fixed LO field power. (b) Measurement of the weak signal field using the resonant EIT-AT splitting technique with $f_{LO} = 3.228$ GHz and $\delta = 75$ kHz. The data are taken with the resonant heterodyne technique (black dots) and EIT-AT splitting in the strong field regime (red dots). The red solid line displays the electric field strength calculated by the equation of $E = F \cdot (30Pg)^{1/2}/d$. The dashed line shows the detectable electric field of $E_{det} = 0.96\ \mu$V/cm. For both the far off-resonant heterodyne technique and the resonant heterodyne technique, the data are interrogated by a spectrum analyzer with a resolution bandwidth of 10 Hz (the measurement time of $T = 0.1$ s) and a video bandwidth of 1 Hz. Each data point is the average of ten independent measurements, and the error bar represents the standard error.

numerically or experimentally.[20,30] As the RF electric field is multi-reflected by the cell wall forming the standing wave inside the cell, the RF field at a given location inside the cell can be larger or smaller than the incident field. The strength of the RF electric field without vapor cell can be calculated using the far-field formula $E_{FF} = \sqrt{30P \cdot g}/d$. In our experiment, $g = 12.20$ (5.18 dB) for 3.228 (2.180 GHz). P is calibrated using a calibrated power meter and the spectrum analyzer to account for the cable loss. The E-field inside the vapor cell E_{tot} is determined from the conventional AT splitting technique using Eq. (2) or AC Stark shifts using Eq. (4). The F factor is obtained by the ratio of E_{tot}/E_{FF}. We obtain the factor $F \approx 1.03$ for 3.228 GHz, and $F \approx 1.20$ for 2.180 GHz in this work. The calculated result is plotted with a red solid line to calibrate the measurements of Fig. 3(a). The measurements demonstrate a linear dependence on P, from which the electric field strength is extracted. The polarizability of the $|60D_{5/2}, m_j = 1/2\rangle$ state is -4.992 GHz · cm^2/V^2 calculated using Alkali-Rydberg-Calculator (ARC).[31] After the calibration, the detectable value of the signal field is down to $E_{det} \simeq 2.25\ \mu$V/cm, which corresponds to a sensitivity of 712 nV cm^{-1} Hz$^{-1/2}$ with the resolution bandwidth of 10 Hz, and the linear response dynamic range is over 65 dB.

For comparison of the performance of the far off-resonant measurement, we do the measurement using the same setup but employing the resonant EIT-AT spectrum technique,[19] where the LO field is resonant with the transition $|60D_{5/2}\rangle \rightarrow |61P_{3/2}\rangle$ with a frequency of 3.228 GHz, and the measurement is displayed in Fig. 3(b). The detectable electric field is down to $E_{det} \simeq 0.96\ \mu$V/cm with a sensitivity of 304 nV cm^{-1} Hz$^{-1/2}$. For more details, see our previous work.[28] From Figs. 3(a) and 3(b), we can see that the off-resonant AC Stark measurement has comparable sensitivity with the resonant EIT-AT measurement achieved using the same system.

It is worth noting that we use AC Stark shift of Eq. (4) to calibrate the RF field of Fig. 3(a) for simplicity, which is valid when the calibration field is less than the field E_{cross} (the first line mixture appears). When the field strength required is larger than E_{cross}, the AC Stark map shows complicated spectral features, including line crossing and avoided crossing,[4] and Eq. (4) is not valid any more. We then need to use the nonperturbative Floquet method to calculate the AC Stark map for calibrating the RF field, where the line mixture is attributed to the contribution of nearby Rydberg states. Due to the n^7 scaling of the polarizability of Rydberg state, the field E_{cross} decreases with n. For this work, the E_{cross} for the 60 $D_{5/2}$ state is ~0.55 V/cm, and the RF field range for calibration of Fig. 3(a) is less than 0.35 V/cm, which is safe for the calibration of the RF field with Eq. (4).

To verify the continuous-frequency measurement property of our system, we do a series of measurements like in Fig. 3(a) but with several far off-resonant RF frequencies. The performance of our Rydberg system at different frequencies is shown in Table I, where we list the detectable RF electric fields with the same resolution bandwidth of 10 Hz. The detectable field is almost same at the RF frequency range of 2–5 GHz, which shows that our method can achieve the continuously tunable measurement of the RF electric field. Our measurement of this work presents the RF frequency range below 5 GHz, which is limited by the RF source we have. In theory, the RF frequency range can be extended to any broad.

Finally, we show our system has an inherent polarization selectivity feature as the response of state with different m_j depends on the polarization of the incident field.[4] The polarization selectivity feature is different from an embedded Rydberg-atom sensor, which has an inherent polarization selectivity feature due to the geometry of the parallel-plate waveguide (PPWG) antenna.[29] Here, we fix the signal field $E_{Sig} = 0.73$ mV/cm and hold the polarization of the LO field along the y-axis, while varying the polarization of the signal field by rotating the antenna of the signal field around the z-axis to study the

TABLE I. The achieved weakest detectable field at different frequencies with the same resolution bandwidth of 10 Hz.

f_{LO} (GHz)	2.18	3.228	4.27	5.18
E_{det} (μV/cm)	2.25	0.96	3.53	8.52

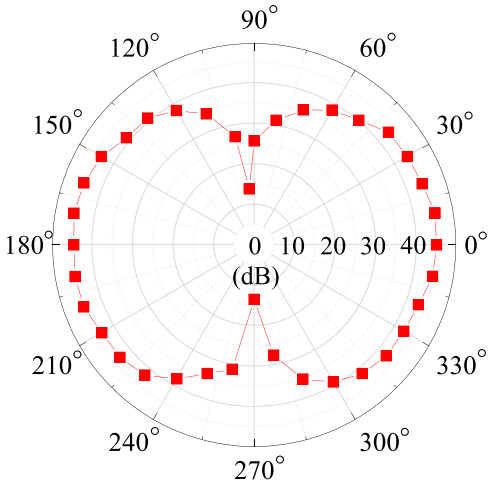

FIG. 4. The measurement of the dependence of output signal of the spectrum analyzer on the angle θ between the LO field and the signal field. The result shows that the isolation for two orthogonal signal fields is up to 32 dB.

polarization selectivity feature. Figure 4 shows the dependence of output signal from the spectrum analyzer on the angle θ between the LO field and the signal field. We can see that when the signal field and the LO field are co-linear polarization, $\theta = 0°$ or 180°, the output signal is 45 dB above the noise. However, when the LO field and signal field are orthogonal, $\theta = 90°$ or 270°, the output signal is 13 dB above the noise. The isolation for two orthogonal signal fields is up to 32 dB.

In this paper, we demonstrated the continuously tunable weak electric field measurement with the RF frequency range of 2–5 GHz using a far off-resonant AC Stark effect in a room-temperature cesium vapor cell. The EIT spectrum is used as an all-optical field probe. The nD Rydberg EIT spectra exhibit m_j dependent AC Stark shifts and splitting at a strong LO field, and the $m_j = 1/2$ Stark level exhibits a high sensitivity to the signal field due to its larger polarizability. We achieve a detectable signal field down to 2.25 μV/cm with a sensitivity of 712 nV cm^{-1} Hz$^{-1/2}$ and a linear dynamic range over 65 dB. We also show the system is enable to detection of polarization of a RF field. It is worth noting that the work here provides the effective method to measure the weak RF field of the continuous RF frequency. In theory, the AC-Stark-based weak field measurement can achieve continuous operation over a large frequency range and detect weak signals with high sensitivity, which has a great prospect in the RF electric field metrology and atom-based quantum communication.

This work was supported by the National Key Research and Development Program of China (No. 2017 YFA0304203), the National Natural Science Foundation of China (Nos. 12120101004, 61835007, and 62175136), the Changjiang Scholars and Innovative Research Team in University of Ministry of Education of China (Grant No. IRT 17R70), and the Fund for Shanxi 1331 Project.

AUTHOR DECLARATIONS

Conflict of Interest

The authors have no conflicts to disclose.

Author Contributions

Jinlian Hu: Data curation (equal); Investigation (equal); Writing – original draft (equal). **Huaqiang Li:** Investigation (equal); Software (equal). **Rong Song:** Software (equal). **Jingxu Bai:** Software (equal); Visualization (equal). **Yuechun Jiao:** Conceptualization (equal); Funding acquisition (equal); Project administration (equal); Supervision (equal); Validation (equal); Writing – review and editing (equal). **Jianming Zhao:** Funding acquisition (equal); Project administration (equal); Supervision (equal); Writing – review and editing (equal). **Suotang Jia:** Project administration (equal).

DATA AVAILABILITY

The data that support the findings of this study are available from the corresponding authors upon reasonable request.

REFERENCES

[1]A. D. Ludlow, M. M. Boyd, J. Ye, E. Peik, and P. O. Schmidt, "Optical atomic clocks," Rev. Mod. Phys. **87**, 637–701 (2015).
[2]B. Patton, O. O. Versolato, D. C. Hovde, E. Corsini, J. M. Higbie, and D. Budker, "A remotely interrogated all-optical ^{87}Rb magnetometer," Appl. Phys. Lett. **101**, 083502 (2012).
[3]T. F. Gallagher, *Rydberg Atoms* (Cambridge University Press, Cambridge, 1994).
[4]Y. Jiao, L. Hao, X. Han, S. Bai, G. Raithel, J. Zhao, and S. Jia, "Atom-based radio-frequency field calibration and polarization measurement using cesium nD_J floquet states," Phys. Rev. Appl. **8**, 014028 (2017).
[5]S. A. Miller, D. A. Anderson, and G. Raithel, "Radio-frequency-modulated Rydberg states in a vapor cell," New J. Phys. **18**, 053017 (2016).
[6]C. G. Wade, N. Šibalić, N. R. de Melo, J. M. Kondo, C. S. Adams, and K. J. Weatherill, "Real-time near-field terahertz imaging with atomic optical fluorescence," Nat. Photonics **11**, 40–43 (2017).
[7]J. A. Sedlacek, A. Schwettmann, H. Kübler, R. Löw, T. Pfau, and J. P. Shaffer, "Microwave electrometry with Rydberg atoms in a vapour cell using bright atomic resonances," Nat. Phys. **8**, 819–824 (2012).
[8]H. Fan, S. Kumar, J. Sedlacek, H. Kübler, S. Karimkashi, and J. P. Shaffer, "Atom based RF electric field sensing," J. Phys. B **48**, 202001 (2015).
[9]J. A. Sedlacek, A. Schwettmann, H. Kübler, and J. P. Shaffer, "Atom-based vector microwave electrometry using rubidium Rydberg atoms in a vapor cell," Phys. Rev. Lett. **111**, 063001 (2013).
[10]H. Q. Fan, S. Kumar, R. Daschner, H. Kübler, and J. P. Shaffer, "Subwavelength microwave electric-field imaging using Rydberg atoms inside atomic vapor cells," Opt. Lett. **39**, 3030–3033 (2014).
[11]C. L. Holloway, J. A. Gordon, A. Schwarzkopf, D. A. Anderson, S. A. Miller, N. Thaicharoen, and G. Raithel, "Sub-wavelength imaging and field mapping via electromagnetically induced transparency and Autler-Townes splitting in Rydberg atoms," Appl. Phys. Lett. **104**, 244102 (2014).
[12]A. K. Robinson, N. Prajapati, D. Senic, M. T. Simons, and C. L. Holloway, "Determining the angle-of-arrival of a radio-frequency source with a Rydberg atom-based sensor," Appl. Phys. Lett. **118**, 114001 (2021).
[13]K. C. Cox, D. H. Meyer, F. K. Fatemi, and P. D. Kunz, "Quantum-limited atomic receiver in the electrically small regime," Phys. Rev. Lett. **121**, 110502 (2018).
[14]Y. Jiao, X. Han, J. Fan, G. Raithel, J. Zhao, and S. Jia, "Atom-based receiver for amplitude-modulated baseband signals in high-frequency radio communication," Appl. Phys. Express **12**, 126002 (2019).
[15]Z. Song, H. Liu, X. Liu, W. Zhang, H. Zou, J. Zhang, and J. Qu, "Rydberg-atom-based digital communication using a continuously tunable radio-frequency carrier," Opt. Express **27**, 8848–8857 (2019).
[16]D. A. Anderson, R. E. Sapiro, and G. Raithel, "An atomic receiver for AM and FM radio communication," IEEE Trans. Antennas Propag. **69**, 2455–2462 (2021).
[17]M. T. Simons, A. H. Haddab, J. A. Gordon, and C. L. Holloway, "A Rydberg atom-based mixer: Measuring the phase of a radio frequency wave," Appl. Phys. Lett. **114**, 114101 (2019).

[18]C. L. Holloway, M. T. Simons, J. A. Gordon, and D. Novotny, "Detecting and receiving phase-modulated signals with a Rydberg atom-based receiver," IEEE Antennas Wireless Propag. Lett. **18**, 1853–1857 (2019).
[19]M. Jing, Y. Hu, J. Ma, H. Zhang, L. Zhang, L. Xiao, and S. Jia, "Atomic superheterodyne receiver based on microwave-dressed Rydberg spectroscopy," Nat. Phys. **16**, 911–915 (2020).
[20]J. A. Gordon, M. T. Simons, A. H. Haddab, and C. L. Holloway, "Weak electric-field detection with sub-1 Hz resolution at radio frequencies using a Rydberg atom-based mixer," AIP Adv. **9**, 045030 (2019).
[21]N. Prajapati, A. K. Robinson, S. Berweger, M. T. Simons, A. B. Artusio-Glimpse, and C. L. Holloway, "Enhancement of electromagnetically induced transparency based Rydberg-atom electrometry through population repumping," Appl. Phys. Lett. **119**, 214001 (2021).
[22]M. T. Simons, A. B. Artusio-Glimpse, C. L. Holloway, E. Imhof, S. R. Jefferts, R. Wyllie, B. C. Sawyer, and T. G. Walker, "Continuous radio-frequency electric-field detection through adjacent Rydberg resonance tuning," Phys. Rev. A **104**, 032824 (2021).
[23]Y.-Y. Jau and T. Carter, "Vapor-cell-based atomic electrometry for detection frequencies below 1 kHz," Phys. Rev. Appl. **13**, 054034 (2020).
[24]D. A. Anderson and G. Raithel, "Continuous-frequency measurements of high-intensity microwave electric fields with atomic vapor cells," Appl. Phys. Lett. **111**, 053504 (2017).
[25]D. H. Meyer, P. D. Kunz, and K. C. Cox, "Waveguide-coupled Rydberg spectrum analyzer from 0 to 20 GHz," Phys. Rev. Appl. **15**, 014053 (2021).
[26]D. J. McCarron, S. A. King, and S. L. Cornish, "Modulation transfer spectroscopy in atomic rubidium," Meas. Sci. Technol. **19**, 105601 (2008).
[27]M. G. Bason, M. Tanasittikosol, A. Sargsyan, A. K. Mohapatra, D. Sarkisyan, R. M. Potvliege, and C. S. Adams, "Enhanced electric field sensitivity of rf-dressed Rydberg dark states," New J. Phys. **12**, 065015 (2010).
[28]L. Hao, Y. Xue, J. Fan, J. Bai, Y. Jiao, and J. Zhao, "Precise measurement of a weak radio frequency electric field using a resonant atomic probe," Chin. Phys. B **29**, 033201 (2020).
[29]M. T. Simons, A. H. Haddab, J. A. Gordon, D. Novotny, and C. L. Holloway, "Embedding a Rydberg atom-based sensor into an antenna for phase and amplitude detection of radio-frequency fields and modulated signals," IEEE Access **7**, 164975–164985 (2019).
[30]A. K. Robinson, A. B. Artusio-Glimpse, M. T. Simons, and C. L. Holloway, "Atomic spectra in a six-level scheme for electromagnetically induced transparency and Autler-Townes splitting in Rydberg atoms," Phys. Rev. A **103**, 023704 (2021).
[31]N. Šibalić, J. D. Pritchard, C. S. Adams, and K. J. Weatherill, "ARC: An open-source library for calculating properties of alkali Rydberg atoms," Comput. Phys. Commun. **220**, 319–331 (2017).